# Collinear laser spectroscopy of radioisotopes of zirconium

Thayer, H. L.; Billowes, J.; Campbell, P.; Dendooven, P.; Flanagan, K. T.; Forest, D. H.; Griffith, J. A.R.; Huikari, J.; Jokinen, A.; Moore, R.

*Published in:*
Journal of Physics G: Nuclear and Particle Physics

*DOI:*
10.1088/0954-3899/29/9/318



*Publication date:*
2003

# Collinear laser spectroscopy of radioisotopes of zirconium

INSTITUTE OF PHYSICS PUBLISHING JOURNAL OF PHYSICS G: NUCLEAR AND PARTICLE PHYSICS

J. Phys. G: Nucl. Part. Phys. **29** (2003) 2247–2262 PII: S0954-3899(03)62271-1

# Collinear laser spectroscopy of radioisotopes of zirconium

**H L Thayer[1], J Billowes[2], P Campbell[2], P Dendooven[3,4], K T Flanagan[2], D H Forest[1], J A R Griffith[1], J Huikari[3], A Jokinen[3], R Moore[2], A Nieminen[3], G Tungate[1], S Zemlyanoi[2] and J Äystö[3]**

[1] School of Physics and Astronomy, The University of Birmingham, Edgbaston, Birmingham B15 2TT, UK
[2] Schuster Laboratory, University of Manchester, Manchester M13 9PL, UK
[3] Department of Physics, University of Jyväskylä, PB 35 (YFL) FIN-40351 Jyväskylä, Finland

E-mail: hlt@np.ph.bham.ac.uk

Received 16 April 2003, in final form 10 June 2003
Published 4 August 2003
Online at stacks.iop.org/JPhysG/29/2247

**Abstract**

Isotope shifts and hyperfine structures have been measured for radioisotopes of ionic zirconium using on-line laser spectroscopy at the IGISOL facility in Jyväskylä, where the installation of an ion beam cooler/buncher has significantly improved the experimental sensitivity. Measurements have been made on all the neutron-deficient isotopes from $^{87}$Zr to $^{90}$Zr, including the isomers $^{87m,89m}$Zr, and the neutron-rich isotopes from $^{96}$Zr to $^{102}$Zr. The change in mean square charge radii between the isotopes and the nuclear moments of the odd isotopes have been extracted. The data show a sudden increase in the mean square charge radius at mass $A = 100$, consistent with an onset of nuclear deformation which has been observed in the gamma ray spectroscopy of isotope chains in this region of the nuclear chart.

## 1. Introduction

High resolution laser spectroscopy is a well-established technique for measuring isotope shifts and hyperfine structures, from which information can be extracted on nuclear properties such as nuclear charge radii, nuclear moments and spins [1, 2]. The high sensitivity of the method makes it suitable for studying the low yields of radioisotopes produced at isotope separators, thus enabling measurement of the properties of nuclei far from stability. Laser spectroscopic measurements now exist for hundreds of isotopes across the nuclear chart, but there are several regions which have remained inaccessible because of problems in the production of ionic beams. The refractory isotopes of the zirconium chain present one such case.

[4] Present address: KVI, Zernikelaan 25, 9747 AA Groningen, Netherlands.

  

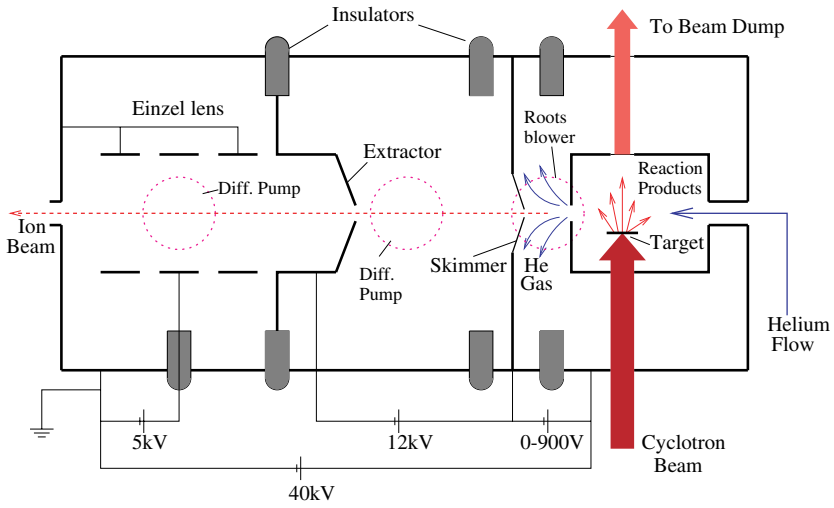


**Figure 1.** The IGISOL (ion guide isotope separator on-line).

The zirconium region of the nuclear chart is of great nuclear physics interest as it shows rapid changes in nuclear deformation on both sides of the $N = 50$ neutron shell closure [3]. There is also evidence for a sudden onset of strong ground state deformation at $A \sim 100$, which has already been observed in the strontium [4] and rubidium [5] chains via isotope shift measurements. Previous laser spectroscopic measurements on zirconium have been restricted to the stable isotopes [6, 7] due to the highly refractory nature of zirconium. The development of the IGISOL (ion-guide isotope separator on-line) facility [8] at the University of Jyväskylä has made it possible to produce ionic beams of refractory isotopes, which are probed using a collinear laser spectroscopy set-up (as described by Levins *et al* [9]). The addition of an ion beam cooler [10] to the beam line has significantly improved the sensitivity of the technique, and has facilitated the production of radioactive beams of zirconium isotopes ideally suited to laser spectroscopic measurements.

This paper describes in full the first laser spectroscopy results for the radioactive isotopes and isomers of zirconium, $^{87,87m,88,89,89m,97-102}$Zr. We also report the introduction of a new technique using bunched ion beams, which has significantly improved the signal to background ratio. The present data were first reported by Campbell *et al* [11] and Forest *et al* [12].

## 2. Experimental method

### *2.1. Laser spectroscopy using the IGISOL*

The IGISOL technique involves thermalizing nuclear reaction products by slowing them in a fast flowing jet of helium gas. A significant fraction (1–10%) of the reaction products remain in the $1^+$ charge state, and these ions are separated from the gas by a skimmer electrode in the jet expansion region (figure 1). The ions are then electrostatically accelerated to 37–40 keV and injected into a mass separator. The advantage of this technique is that it can be applied to any element, including refractory metals, and the fast extraction time allows beams of ions with half-lives as short as a millisecond to be produced without significant loss through decay [13]. After mass separation, the ion beam is transported to the laser-ion interaction region, where it is collinearly overlapped with a fixed frequency laser beam. An additional accelerating voltage

is applied to the interaction region to Doppler-tune the ions onto resonance with the laser, and the scattered photons are imaged onto a Hamamatsu R5900P-03-L16 photomultiplier tube. The photomultiplier counts a continuous background of scattered, non-resonant laser light, which must be suppressed in order to detect any signal from the ionic resonances. Previous measurements [9, 14] have used a photon-ion coincidence requirement to reject background.

A major disadvantage of the IGISOL technique is that the ion beam has a relatively large energy spread (10–150 eV) [15], caused by collisions with gas molecules during electrostatic extraction from the helium. Both the energy spread and the ion yield increase with the skimmer voltage, but the sensitivity of laser spectroscopy at the IGISOL is critically dependent on the quality of the beam. Therefore, previous laser spectroscopic measurements [16] have had to sacrifice beam intensity by running at low skimmer voltage to minimize the energy spread of the beam.

### *2.2. The ion beam cooler/buncher*

An ion beam cooler [10] was developed to eliminate the large energy spread of the ion beam and to improve the beam emittance, thus increasing the efficiency of laser spectroscopy. The device consists of a gas-filled radio-frequency quadrupole (RFQ) which cools the ions via collisions with the helium buffer gas. After mass separation, the ions are injected into the cooler and transported along its length by a weak axial field. Within the RFQ, the ions are thermalized and squeezed onto the quadrupole axis, and they exit with a significantly reduced energy spread of $<1$ eV, and an emittance of $3\pi$-mm-mrad. The quality of the resulting ion beam is independent of the conditions in the IGISOL, thus allowing the IGISOL parameters to be optimized to give the maximum ion yield without compromising on the beam quality. The cooler can also be operated as an ion trap capable of accumulating ions for several hundred milliseconds, and releasing them in short bunches of 10–20 $\mu$s [17, 18].

The bunching capability of the cooler has led to the introduction of a new way of performing laser spectroscopy using bunched ion beams. A significant reduction in photon background can be achieved by electronically gating the photomultiplier signal such that photon events are only accepted if they arrive while an ion bunch is in front of the detector. This allows a suppression of the background by a factor of $S = t_{\mathrm{acc}}/w$, where $t_{\mathrm{acc}}$ is the accumulation time in the cooler, $w$ is the width of the electronic gate and typically $S \sim 10^4$ [18].

### *2.3. Off-line tests*

The IGISOL can be used to produce stable ion beams by placing a discharge source within the IGISOL chamber. A sample of stable material is placed at the cathode of the discharge source and an applied voltage of $\sim$500 V causes sputtering and ionization of the sample [16]. The ions are extracted from the IGISOL in the same way as for on-line running, producing an ion beam with an intensity of the order of 1 nA which is used to optimize the apparatus prior to an on-line experiment.

Preliminary off-line tests were carried out using stable zirconium beams in order to optimize the cooler parameters and determine the best ionic transitions to be used during the on-line experiments. Various ZrII transitions in the UV were studied by Doppler tuning the ions onto resonance with the frequency-doubled output of a Spectra Physics 380 dye laser. In each case, frequency stabilization was achieved by electronically locking the fundamental laser output to a nearby absorption line of molecular iodine. Of the studied transitions, those at 309.9 nm ($4d^2 5s\,{}^4\mathrm{F}_{3/2} - 4d^2 5p\,{}^4\mathrm{D}_{3/2}$) and 327.2 nm ($4d^2 5s\,{}^4\mathrm{F}_{3/2} - 4d^2 5p\,{}^4\mathrm{F}_{5/2}$) were observed to give the best spectroscopic efficiencies. Rhodamine B dye provided the required

fundamental output for the 309.9 nm transition, with the laser locked to an iodine absorption line at 16 112.8784 $cm^{-1}$ [19]. A mixture of rhodamine 6G and rhodamine 640 dyes was used for the 327.2 nm transition, with the fundamental output locked to 15 261.6804 $cm^{-1}$. Continuous ion beams were used to obtain measurements of the hyperfine structure of $^{91}$Zr, and isotope shifts between all of the stable isotopes.

Further tests using bunched ion beams showed the spread in release times of the ions from the cooler to be $\sim$15 $\mu$s, and the optimum ion storage time to be 200 ms. Longer storage times resulted in significant losses in spectroscopic efficiency caused by the formation of charged molecules in the cooler. Time of flight spectra taken for the ions exiting the cooler showed evidence that these molecules could be $Zr^{+}(H_2O)_n$ complexes [11].

The off-line tests also served to deposit a layer of stable zirconium onto the skimmer plate of the IGISOL, which was subsequently used as a discharge source to provide a stable calibration beam of $^{90}$Zr during on-line running.

### *2.4. On-line measurements*

Neutron-deficient radioisotopes of zirconium were produced on-line using $^{89}$Y(p, $x$n)$^{90-x}$Zr fusion-evaporation reactions with a proton beam flux of 10 $\mu$A incident on a 1 mg $cm^{-2}$ thick target. A proton beam energy of 16 MeV was used to produce beams of $^{88,89,89m}$Zr, and increased in energy to 40 MeV to produce $^{86,87,87m,88}$Zr. Total ion rates were monitored using a microchannel plate detector positioned downstream of the laser interaction region, and a measurement of the radioactive fraction was obtained using a gamma-ray counting station positioned at the exit of the cooler. Ion production rates after cooling ranged from $\sim$300 $s^{-1}$ for the isomeric states $^{87m,89m}$Zr, up to $\sim$5000 $s^{-1}$ for $^{89}$Zr. The ions were brought onto resonance with the 309.9 nm transition, using an incident laser power of $\sim$1 mW. Stable calibration beams of up to $\sim 10^4$ ions $s^{-1}$ of $^{90}$Zr were produced by increasing the voltage on the skimmer (which had acquired a coating of stable zirconium during the off-line running of the discharge source) until it began to discharge. As the stable beams were emitted with a slightly lower energy than those produced via nuclear reactions, a compensatory adjustment of the IGISOL extraction voltage was required to bring the ions to the required energy for injection into the cooler. Since the energy of the cooled ion beam is independent of the ion source conditions, this adjustment in voltage did not affect the final energy of the beam. The measurement of the resonance position of $^{90}$Zr served as a reference point to link the on-line measurements of the neutron-deficient isotopes to the off-line measurements of the stable isotopes.

Proton-induced fission of $^{238}$U in a natural uranium target was used to produce the neutron-rich isotopes from $^{96}$Zr to $^{102}$Zr, using a 3.5 $\mu$A beam of 25 MeV protons. Ion production rates ranged from $\sim$500 $s^{-1}$ for the stable calibration isotope, $^{96}$Zr, up to $\sim$3000 $s^{-1}$ for $^{100}$Zr, the most strongly produced isotope. Due to problems encountered with the rhodamine B dye during the neutron-deficient measurements, the studied transition was changed to 327.2 nm for the neutron-rich isotopes.

Throughout both the on-line experiments, the cooler was used to bunch the ion beam and electronic gating was used to reject the photon background, which ranged from 300 to 500 $s^{-1}$ $mW^{-1}$. In the light of off-line tests, the ions were stored in the cooler for 200 ms and two photon collection gates of 10 and 20 $\mu$s per ion bunch were used, giving a total background suppression of $2 \times 10^4$ and $1 \times 10^4$, respectively. The experimental results showed that the 10 $\mu$s window was sufficiently long to collect most of the resonant counts. Many scans of approximately 2 h duration were taken for each isotope. The tuning voltage was scanned over a range of up to 200 V, where 1 V corresponds to $\sim$11 MHz in frequency space. The magnitude

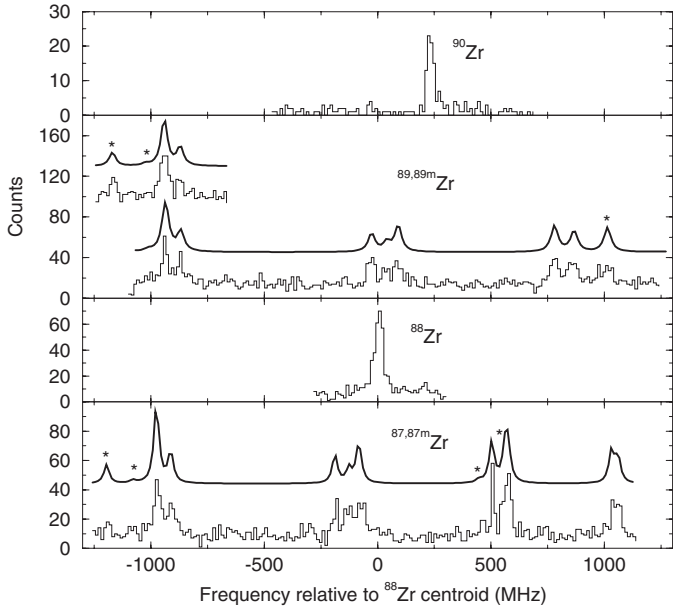


**Figure 2.** Spectra obtained for the neutron-deficient isotopes of zirconium. Fits to $^{87,87m}$Zr and $^{89,89m}$Zr are shown above the data. Isomer components are marked with an asterisk.

of the kinematic voltage shift, due to heavier isotopes requiring a greater accelerating voltage to bring them onto resonance, was approximately 400 V per mass unit.

Scans were alternated with measurements on a reference isotope ($^{88}$Zr for the neutron-deficient isotopes, and $^{100}$Zr for the neutron-rich) in order that any drifts in centroid positions could be detected and corrected for. Centroid shifts of up to 2 V were observed between blocks of data taken at different times. Since drifts in the cooler and tuning voltages could be monitored to an accuracy of 0.1 V, these shifts were most likely due to changes in the laser locking frequency. Hyperfine structure was observed for all of the odd mass isotopes, including the isomeric states $^{87m,89m}$Zr. Unfortunately, no data were obtained for $^{86}$Zr due to contamination of the beam with large amounts of krypton, which had been used to provide a mass calibration [12]. The summations of the spectra for each mass are shown in figures 2 and 3, where the abscissae have been converted from acceleration voltages to Doppler corrected frequencies relative to the resonance positions of the reference isotopes, $^{88}$Zr and $^{100}$Zr.

## 3. Data analysis

The experimental spectra (figures 2 and 3) show shifts in the centroids of the ionic resonances between different isotopes due to differences in their mass and mean square charge radii. The odd mass isotopes display hyperfine structure resulting from the nuclear multipole moments perturbing the electronic structure. The hyperfine spectra seen for $^{87}$Zr and $^{89}$Zr are combinations of components from both the ground and isomeric states.

The hyperfine splitting relative to the position of the centroid of an ionic state is given by [20],

$$E_{hf} = \frac{A}{2}K + \frac{B}{4}\frac{\frac{3}{2}K(K+1) - 2I(I+1)J(J+1)}{I(2I-1)J(2J-1)} \tag{1}$$

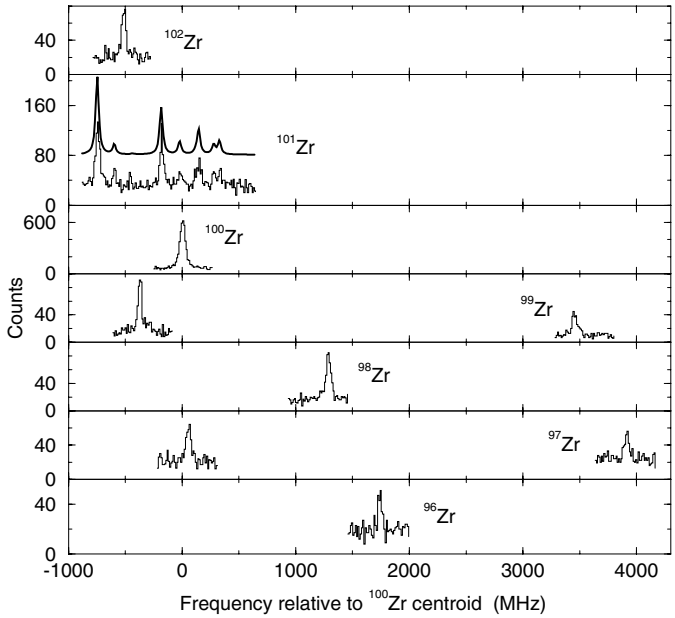


**Figure 3.** Spectra obtained for the neutron-rich isotopes of zirconium. The fit to $^{101}$Zr is shown above the data.

where $K = [F(F+1) - I(I+1) - J(J+1)]$, $I$ is the nuclear angular momentum, $J$ is the electronic angular momentum and $F$ is the total angular momentum. The factors $A$ and $B$ are the magnetic dipole and electric quadrupole hyperfine parameters, and are related to the nuclear moments by,

$$A = \frac{\mu_I B_e}{IJ} \qquad \text{and} \qquad B = eQ_s \left\langle \frac{\partial^2 V_e}{\partial z^2} \right\rangle \tag{2}$$

where $\mu_I$ is the nuclear magnetic dipole moment, $Q_s$ is the spectroscopic quadrupole moment and $B_e$ and $\partial^2 V_e/\partial z^2$ are the magnetic field and electric field gradient produced at the nucleus by the atomic electrons. Unknown nuclear moments can be deduced from hyperfine structure measurements via,

$$\mu_1 = \frac{A_1 I_1}{A_2 I_2}\mu_2(1+\Delta) \qquad \text{and} \qquad Q_{s1} = \frac{B_1}{B_2}Q_{s2} \tag{3}$$

where 1 and 2 refer to two different isotopes, and isotope 2 has known nuclear moments. $\Delta$ is the hyperfine anomaly, and is a small correction which accounts for isotopic differences in the distribution of nuclear magnetization over the nuclear volume. Corrections due to the hyperfine anomaly are typically $<1\%$, although anomalies of up to $\sim 10\%$ have been observed in some cases [21].

The isotope shift between two isotopes with atomic masses $A$ and $A'$ is given by $\delta\nu_{IS}^{A,A'} = \nu^{A'} - \nu^{A}$, and to an excellent approximation [22], the shift can be split into two components, the mass shift $\left(\mathrm{MS}_i^{A,A'}\right)$ and the field shift $\left(\mathrm{FS}_i^{A,A'}\right)$, where

$$\delta\nu_i^{A,A'} = \mathrm{MS}_i^{A,A'} + \mathrm{FS}_i^{A,A'} = \left(\frac{A'-A}{AA'}\right) M_i + F_i \lambda^{A,A'} \tag{4}$$

and $\lambda^{A,A'}$ is a nuclear parameter which is linearly proportional to the change in the nuclear mean square charge radius, $\delta\langle r^2\rangle^{A,A'}$. With the exception of very heavy nuclei, the approximation

**Table 1.** Isotope shifts, hyperfine parameters and nuclear spins determined for the ionic transition at 309.9 nm. Statistical errors are given in round brackets and systematic uncertainties are shown in square brackets.

| $A$ | $I$ | $A'$ | $\nu^{A'} - \nu^{A}$ (MHz) | $A_l$ (MHz) | $B_l$ (MHz) |
|---|---|---|---|---|---|
| 87 | 9/2 | 90 | +250(8)[3] | +127.2(2) | +35.3(35) |
| 87 m | 1/2 | 90 | +303(9)[3] | −820.5(27) | 0 |
| 88 | 0 | 90 | +203(7)[3] | 0 | 0 |
| 89 | 9/2 | 90 | +58(8)[1] | +148.6(5) | +23(8) |
| 89 m | 1/2 | 90 | +7(10)[0.1] | −1016.9(31) | 0 |
| 91 | 5/2 | 90 | +178(3)[2] | +333.3(3) | −14.7(8) |
| 92 | 0 | 90 | +450(3)[5] | 0 | 0 |
| 94 | 0 | 90 | +768(3)[8] | 0 | 0 |
| 96 | 0 | 90 | +978(3)[10] | 0 | 0 |

**Table 2.** Isotope shifts, hyperfine parameters and spins determined for the ionic transition at 327.2 nm. Statistical errors are given in round brackets and systematic uncertainties are shown in square brackets.

| $A$ | $I$ | $A'$ | $\nu^{A'} - \nu^{A}$ (MHz) | $A_l$ (MHz) | $B_l$ (MHz) |
|---|---|---|---|---|---|
| 97 | 1/2 | 96 | +165(9)[2] | +1197.4(17) | 0 |
| 98 | 0 | 96 | +447(10)[4] | 0 | 0 |
| 99 | 1/2 | 96 | +609(9)[6] | +1189.1(3) | 0 |
| 100 | 0 | 96 | +1726(9)[17] | 0 | 0 |
| 101 | 3/2 | 96 | +2034(9)[20] | +115.9(4) | +67.8(27) |
| 102 | 0 | 96 | +2255(11)[23] | 0 | 0 |
| 91 | 5/2 | 90 | +192(4)[2] | +333.3(3) | −14.7(8) |
| 92 | 0 | 90 | +494(4)[5] | 0 | 0 |
| 94 | 0 | 90 | +823(4)[8] | 0 | 0 |
| 96 | 0 | 90 | +1033(4)[10] | 0 | 0 |

$\lambda^{A,A'} \approx \delta\langle r^2\rangle^{A,A'}$ is valid. $M_i$ and $F_i$ are atomic factors which must be evaluated or calibrated in order to extract the nuclear information. A standard technique for deducing these parameters is the King plot method [22], which allows optical measurements to be combined with non-optical data to calibrate the atomic factors for a transition.

A chi-squared minimization routine was used to fit Lorentzian profiles to the resonance peaks in the experimental spectra (figures 2 and 3). In the case of the odd isotopes, a global fit to the whole of the hyperfine structure was performed for each isotope. The ratios of the upper and lower state $A$ and $B$ factors were constrained to be equal to the ratios measured for $^{91}$Zr during off-line tests (with the assumption of no hyperfine anomaly), where $(A_l/A_u)_{327.7} = -2.462(4)$, $(B_l/B_u)_{327.2} = +1.91(53)$, $(A_l/A_u)_{309.9} = -13.917(77)$ and $(B_l/B_u)_{309.9} = -2.72(29)$. Isotope shifts, hyperfine parameters and nuclear spins were determined from the fits to the data. These values are given in tables 1 and 2, where the results of the off-line measurements on the stable isotopes of zirconium are also included. Statistical errors arise from uncertainties in the fitting of the spectra. In addition, systematic errors have been assigned to the isotope shifts to account for possible uncertainties in the calibration of the total acceleration voltage. Off-line measurements indicated the magnitude of this uncertainty to be $\sim$1%.

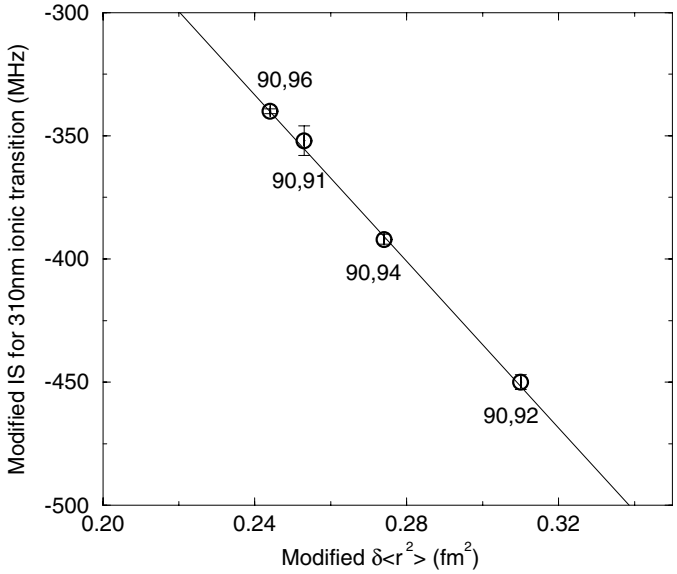


**Figure 4.** King plot of 309.9 nm ionic Zr isotope shifts against the $\delta\langle r^2\rangle$ evaluations of Fricke *et al* [25] and Campbell *et al* [7]. The 5% systematic errors on the $\delta\langle r^2\rangle$ values are not shown.

Prior to the current measurements, only tentative assignments of the spins of $^{87,87m,99,101}$Zr had been made. As discussed by Campbell *et al* [11] and Forest *et al* [12], the fits to the hyperfine structure of these isotopes ruled out alternative spin assignments and confirmed the suggested assignments to be correct. The spins determined for the other odd isotopes are consistent with existing assignments.

The atomic factors required to extract the changes in mean square charge radii from the isotope shift measurements were evaluated using the King plot method. King's method involves modifying a set of isotope shifts and $\delta\langle r^2\rangle$ values by a factor, $\mu$, which removes the mass dependence, where

$$\mu = \frac{AA'}{A'-A}\,\frac{A'_{\rm ref}-A_{\rm ref}}{A_{\rm ref}A'_{\rm ref}} \tag{5}$$

and $A_{\rm ref}$ and $A'_{\rm ref}$ are a chosen pair of reference isotopes. Modified isotope shifts are then plotted against modified $\delta\langle r^2\rangle$ for different pairs of isotopes. In most cases, the locus of the points forms a straight line[5] whose gradient and intercept are directly related to the atomic factors $F_i$ and $\mathrm{MS}_i^{A_{\rm ref},A'_{\rm ref}}$.

The atomic factors in equation (4) were evaluated via King plots of the stable isotope shift measurements for the two transitions, against the $\delta\langle r^2\rangle$ values of Fricke *et al* [25] and Campbell *et al* [7]. Fricke *et al* used a combination of optical, muonic and electronic scattering data to obtain values of $\delta\langle r^2\rangle$ between the stable even isotopes. Campbell *et al* extended the data to include a value for $\delta\langle r^2\rangle^{90,91}$, derived from optical measurements. Figure 4 shows a King plot of the modified isotope shifts for the 309.9 nm ionic line, against the modified mean square charge radii. The 5% systematic errors on the $\delta\langle r^2\rangle$ values are not shown in the plot. Fitting a straight line to the data allowed the atomic factors to be obtained for the two measured ionic transitions. The parameters were found to be $F_{309.9} = -1690(41)$ MHz fm$^{-2}$

[5] Deviations from the straight line rule have been observed in samarium isotopes by Griffith *et al* [23, 24].

**Table 3.** Magnetic moments, spectroscopic quadrupole moments and changes in mean square charge radii of the measured zirconium isotopes. Statistical errors are given in round brackets and systematic uncertainties are shown in square brackets. As discussed in the text, the systematic uncertainties on $\mu_I$ account for possible effects of the hyperfine anomaly.

| $A$ | $N$ | $I^\pi$ | $\mu_I$ ($\mu_N$) | $Q_s$ (b) | $\delta\langle r^2\rangle^{N=50,N}$ (fm$^2$) |
|---|---|---|---|---|---|
| 87 | 47 | $9/2^+$ | −0.895(2)[3] | +0.423(48) | 0.080(4)[8] |
| 87 m | 47 | $1/2^-$ | +0.642(2)[14] | 0 | 0.111(5)[8] |
| 88 | 48 | $0^+$ | 0 | 0 | 0.075(4)[7] |
| 89 | 49 | $9/2^+$ | −1.046(4)[2] | +0.275(97) | 0.012(5)[8] |
| 89 m | 49 | $1/2^-$ | +0.795(3)[15] | 0 | −0.018(6)[8] |
| 91 | 51 | $5/2^+$ | −1.30362(2)[a] | −0.176(3)[b] | 0.128[6][c] |
| 92 | 52 | $0^+$ | 0 | 0 | 0.310[16][d] |
| 94 | 54 | $0^+$ | 0 | 0 | 0.537[27][d] |
| 96 | 56 | $0^+$ | 0 | 0 | 0.702[35][d] |
| 97 | 57 | $1/2^+$ | −0.937(2)[3] | 0 | 0.813(4)[45] |
| 98 | 58 | $0^+$ | 0 | 0 | 0.981(5)[43] |
| 99 | 59 | $1/2(^+)$ | −0.930(1)[3] | 0 | 1.090(4)[43] |
| 100 | 60 | $0^+$ | 0 | 0 | 1.666(4)[41] |
| 101 | 61 | $3/2(^+)$ | −0.272(1)[7] | +0.812(56) | 1.845(4)[41] |
| 102 | 62 | $0^+$ | 0 | 0 | 1.981(5)[42] |

[a] Results of [26].
[b] Results of [27].
[c] Results of [7].
[d] Results of [25].

and $\mathrm{MS}^{90,92}_{309.9} = +72(11)$ MHz for the 309.9 nm transition, and $F_{327.2} = -2039(41)$ MHz fm$^{-2}$ and $\mathrm{MS}^{90,92}_{327.2} = +139(11)$ MHz for the 327.2 nm transition, where the errors arise from uncertainties in the straight line fits to the data. As expected, the parameters for the 309.9 nm transition show good agreement with those calculated by Campbell *et al* [7]. The parameters were used to separate the mass and field shift contributions to the total isotope shifts, enabling the changes in mean square charge radii to be extracted from the field shifts. Table 3 shows the values of $\delta\langle r^2\rangle$ extracted from the measured shifts. Statistical and systematic errors are given separately, where the systematic errors originate from the uncertainties in the atomic parameters, $M_i$ and $F_i$.

In order to extract the nuclear moments from the measured hyperfine parameters, $B_e$ and $\partial^2 V_e/\partial z^2$ were calibrated using the known isotopic moments for $^{91}$Zr [26, 27], with the assumption of no hyperfine anomalies. Allowance was made for the anomalies being non-negligible by estimating their possible magnitude using the Moskowitz–Lombardi rule [21]. This is an empirical rule which was established for the mercury isotope chain, and relates the $s$-electron hyperfine anomalies, $\Delta_s^{A,A'}$, and nuclear magnetic moments by

$$\Delta_s^{A,A'} = \alpha_s \left( \frac{1}{\mu_A} - \frac{1}{\mu_{A'}} \right) \tag{6}$$

where $\alpha_s$ is a constant whose magnitude is specific to the isotope chain. This relation was used to obtain estimates of the anomalies in zirconium by using the measured hyperfine anomaly in rubidium, $\Delta^{85,87} = 0.350(3)\%$ [21], to calibrate $\alpha_s$ under the assumption that the $p$-electron contribution to the anomaly is negligible. The extracted values for the nuclear moments are given in table 3, where the estimated anomalies have been assigned as systematic errors on the measured moments.

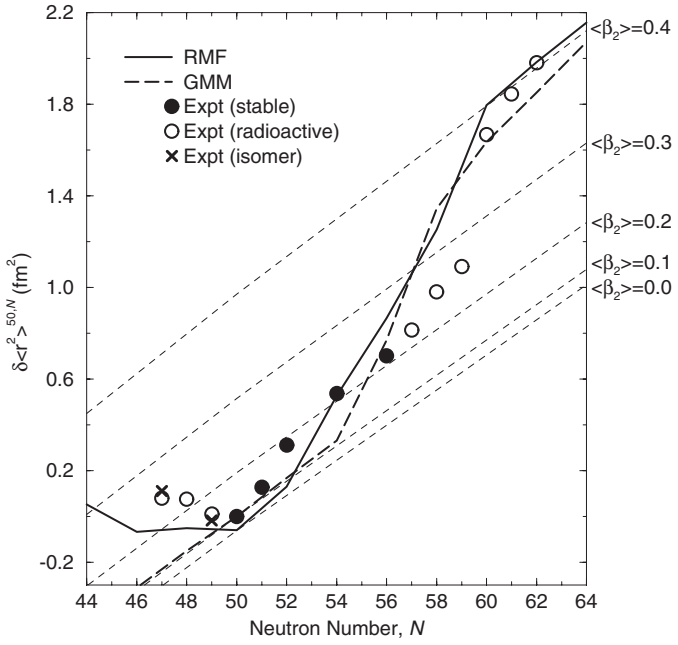


**Figure 5.** Variation of $\delta\langle r^2\rangle$ with neutron number. Error bars generally lie within the experimental points, and are not shown. The predictions of the relativistic mean field theory (RMF) [35] and global macroscopic–microscopic calculations (GMM) [34] are included for comparison. The dashed straight lines show the predictions of the droplet model [28] (using the parameter set of Berdichevsky and Tondeur [29]) for different values of the quadrupole deformation parameter, $\langle\beta_2\rangle$. Droplet model and GMM predictions are normalized to the experimentally determined value of $\langle\beta_2^2\rangle^{1/2} = 0.1$ [30] for $^{90}$Zr.

## 4. Discussion

### *4.1. Changes in mean square charge radii*

The variations in the mean square charge radii, $\delta\langle r^2\rangle$, with neutron number for the measured isotopes of zirconium are shown in figure 5, in which the $\delta\langle r^2\rangle$ values are given relative to $^{90}$Zr. Dashed straight lines show the predictions of the droplet model [28] for different values of the quadrupole deformation parameter, $\langle\beta_2\rangle$. The revised parameter set of Berdichevsky and Tondeur [29] was used in the droplet model calculations. All predictions are normalized to the value of $\langle\beta_2^2\rangle^{1/2} = 0.1$ derived from B(E2) measurements on $^{90}$Zr [30], and indicate how the mean square charge radius changes with the nuclear deformation. The mean square charge radius is smallest at the $N = 50$ neutron shell closure where the nucleus is approximately spherical in shape, and increases rapidly on either side of the shell closure. The sudden increase in the charge radius at $N = 60$ can be attributed to the predicted shape change in this region, which originates from the breakdown of the stabilizing semi-magic proton shell closure at $Z = 40$ [31]. This sudden onset of strong deformation has already been observed in the gamma ray spectroscopy [32] of isotope chains in this region of the nuclear chart. The zirconium mean square charge radii show very similar behaviour to the neighbouring strontium isotones [4], which also have a closed proton sub-shell ($Z = 38$). An interesting feature is observed in the nuclear sizes of the two zirconium isomers on the neutron-deficient side, where in $^{87}$Zr the isomeric state is larger than the ground state, but the opposite is true

for $^{89}$Zr. A similar trend occurs in the mean square charge radii of the neighbouring isomers, $^{85m,87m}$Sr [4] and $^{83m,85m}$Kr [33]. The data show a normal odd–even stagger in the isotopes from $^{87}$Zr to $^{100}$Zr, where the odd isotopes have smaller charge radii than the average of their even-$N$ neighbours. This trend appears to reverse at $^{101}$Zr, whose nuclear size is slightly larger than the average of the two neighbouring even isotopes. Odd–even staggering is observed in all isotope chains throughout the nuclear chart, but as yet there is no satisfactory general quantitative explanation for its occurrence.

Figure 5 also includes the $\delta\langle r^2\rangle$ predictions of two theoretical models. Global macroscopic–microscopic calculations (GMM) [34] include theoretical values for the $\beta_2$ deformation, but the agreement with the data is poor. The relativistic mean field theory (RMF) [35] shows better agreement and reproduces the behaviour at the shell closure, but fails to predict the sudden increase in the mean square charge radius at $N = 60$.

### *4.2. Nuclear moments and spins*

The moments and spins measured for the odd mass isotopes and isomers are given in table 3. A comparison of the magnetic dipole moments with the single-particle predictions of the shell model (Schmidt predictions) can be used to infer the degree of configuration mixing involved in the states [2]. The magnetic moments of the spin $I = 9/2$ $^{87,89}$Zr ground states are lower in magnitude than the Schmidt estimate of $-1.91\,\mu_N$ for a $g_{9/2}$ neutron, as expected from the quenching effects of configuration mixing in the states. However, the Schmidt estimate of +0.636 $\mu_N$ for a $p_{1/2}$ neutron is very close to the measured value of +0.642(2) $\mu_N$ for $^{87m}$Zr, which suggests that the isomeric state shows strong single particle behaviour. This is very similar to the magnetic moment measured for the strontium isotone, where $\mu(^{85m}\mathrm{Sr}) =$ +0.600(4) $\mu_N$ [4]. $^{89m}$Zr has a magnetic moment of +0.795(3) $\mu_N$, which is significantly larger than the $p_{1/2}$ Schmidt estimate, and is in contrast to the case in the isotone $^{87m}$Sr, whose magnetic moment of +0.624(4) $\mu_N$ [4] lies close to the single-particle estimate. However, the zirconium isomers do follow the general trend seen in $^{83m,85m,87m}$Sr, where a progressive decrease in magnetic moment is observed as neutrons are removed. Both isomeric states in Zr involve the excitation of a neutron from the $2p_{1/2}$ orbit to the $1g_{9/2}$ sub-shell, leaving a $2p_{1/2}$ hole state.

On the neutron-rich side, the $^{97,99}$Zr ($I = 1/2$) isotopes have almost identical magnetic moments, which suggest that $^{99}$Zr shares the same $\nu 3s_{1/2}$ configuration as $^{97}$Zr [36]. The magnetic moment of $^{101}$Zr ($-0.272(1)[7]$ $\mu_N$) is extremely small compared to the Schmidt estimate of $-1.91$ $\mu_N$, and indicates that a considerable degree of configuration mixing is involved, due to the collectivity of the state.

### *4.3. Nuclear deformation*

The measured values of the mean square charge radii and quadrupole moments may be used to obtain model-dependent values of the quadrupole deformation parameter. A comparison with deformation parameters derived from B(E2) measurements can then yield valuable nuclear structure information.

Values of the *static* quadrupole deformation parameter, $\langle\beta_2\rangle$, may be extracted from the measured spectroscopic quadrupole moments, $Q_s$. The quadrupole deformation parameter can be related to the intrinsic quadrupole moment, $Q_o$, by the first-order approximation,

$$Q_o = \frac{5Z\langle r^2\rangle_s}{\sqrt{5\pi}}\langle\beta_2\rangle(1 + 0.36\langle\beta_2\rangle) \tag{7}$$

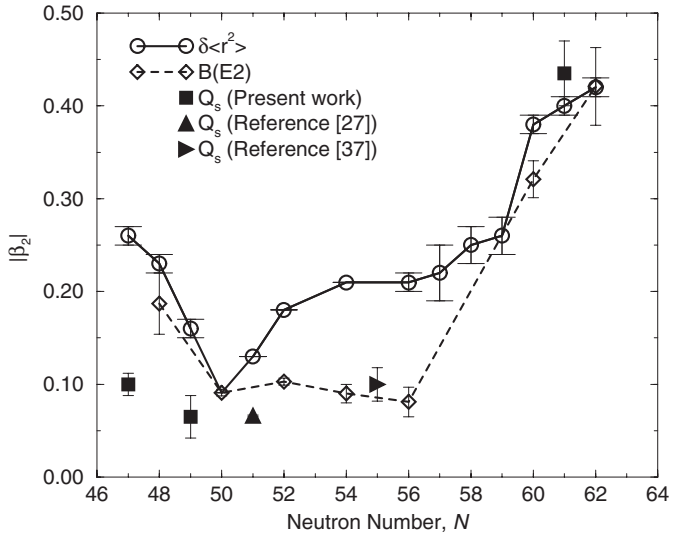


**Figure 6.** Variation of the quadrupole deformation parameter, $|\beta_2|$, with neutron number. The parameters extracted from mean square charge radii, quadrupole moments and B(E2) values [30] are given, where open points denote rms deformation parameters ($\langle\beta_2^2\rangle^{1/2}$). Square points represent values of $|\beta_2|$ extracted from the quadrupole moments measured in this work, and triangles denote values extracted from the measurements of $Q_s(^{91}\mathrm{Zr})$ [27], and $Q_s(^{95}\mathrm{Zr})$ [37].

where $\langle r^2\rangle_s$ is the mean square charge radius of the corresponding spherical nucleus, and is calculated using the droplet model [28]. In the strong coupling limit, the intrinsic and spectroscopic quadrupole moments are related by

$$Q_s = Q_o\left[\frac{3\Omega^2 - I(I+1)}{(I+1)(2I+3)}\right] \tag{8}$$

where $\Omega$ is the projection of the nuclear spin along the nuclear symmetry axis, and for ground states of well deformed nuclei, $\Omega = I$.

Similarly, the root mean square (rms) deformation parameter, $\langle\beta_2^2\rangle^{1/2}$, may be extracted from measurements of mean square charge radii using the approximation given in [1],

$$\langle r^2\rangle = \langle r^2\rangle_s\left(1 + \frac{5}{4\pi}\langle\beta_2^2\rangle\right) + 3\sigma^2 \tag{9}$$

where $\sigma$ is the nuclear diffuseness parameter [28] and is assumed to be constant for all nuclei. $\langle\beta_2^2\rangle^{1/2}$ is a *dynamic* deformation parameter, which is sensitive to both the static deformation, and the effect of collective nuclear vibrations on the nuclear shape.

The quadrupole deformation parameters extracted from the mean square charge radii and the quadrupole moments are given in figure 6, where they are compared with values of $\langle\beta_2^2\rangle^{1/2}$ extracted from B(E2) measurements [30]. Also included are the values of $|\beta_2|$ extracted from non-optical measurements of the quadrupole moment, where $Q_s(^{91}\mathrm{Zr}) = -0.176(3)$ b [27] and $Q_s(^{95}\mathrm{Zr}) = (+)0.29(5)$ b [37]. In the $50 < N < 60$ region, there is a significant discrepancy between the $\langle\beta_2^2\rangle^{1/2}$ values extracted from $\delta\langle r^2\rangle$ and B(E2) measurements. The differences are much larger than the experimental errors and arise from the model approximations made in extracting $\langle\beta_2^2\rangle^{1/2}$ from $\langle r^2\rangle$ and B(E2). In the case of $\langle r^2\rangle$, the effect of the surface diffuseness on the charge radius has been assumed to be constant for all isotopes. This

approximation is valid under the assumption that changes in the nuclear deformation dominate the changes in mean square charge radii. However, the surface diffuseness term may have some isotopic dependence, which could be providing a significant contribution to changes in $\langle r^2 \rangle$. Additionally, in the extraction of $\langle \beta_2^2 \rangle^{1/2}$ from B(E2) values, the sum of B(E2) strengths over all excited $2^+$ states is assumed to be dominated by that of the first state, and contributions from higher lying $2^+$ states are ignored. This is an assumption which is only strictly true for purely vibrational or rotational nuclei [1].

In the region beyond the $N = 60$ shape change, where strong quadrupole deformation sets in, the approximations improve and the deformation parameters derived from the two different methods become more compatible. In this region, the rms deformation parameters also show good agreement with the static deformation parameter extracted from the measured quadrupole moment for $^{101}$Zr. This agreement suggests that the nucleus takes on a rigid, statically-deformed shape above $N = 60$. Below $N = 50$, the agreement between the static and dynamic deformation parameters is poorer. In this region the nucleus has a softer shape, where collective vibrations contribute to the rms deformation. This vibrational contribution to the nuclear size is consistent with the normal odd–even staggering seen in the mean square charge radii. Qualitative descriptions of the normal odd–even stagger suggest that the odd neutron stabilizes the nuclear shape by pushing vibrational states to higher energy [2]. Thus for odd-$N$ nuclei, the dynamic contribution to the mean square charge radius is reduced compared to the neighbouring even-$N$ isotopes. Odd–even staggering has also been interpreted in terms of a decrease in the surface diffuseness, caused by the odd neutron effectively blocking the scattering of neutron pairs into orbits near the Fermi level.

In the transitional region, $50 < N < 60$, it is more difficult to draw conclusions about the behaviour of the nuclear shape, due to the discrepancies between B(E2) and mean square charge radii measurements. Similar discrepancies in the strontium chain have been considered by Mach *et al* [38], who concluded that the effect of octupole vibrations could account for the differences. As discussed by Campbell *et al* [11], this explanation fails to account for the discrepancies seen in the zirconium chain, where the contributions of higher lying $2^+$ states to the B(E2) strength may be most significant. Future optical measurements of $^{93,95}$Zr, yielding static ground state deformation parameters, will give a better indication of the systematics of the transitional region.

Previous studies [38] of the $A \sim 100$ region in strontium and zirconium have suggested that the transition from a spherical to a well deformed ground state is very sudden, involving the coexistence of spherical and strongly deformed shapes. Lhersonneau *et al* [31] postulated that well deformed excited configurations in $^{96,97}$Sr and $^{98,99}$Zr are lowered in energy towards $N = 60$, where they become ground states. However, recent gamma ray measurements by Urban *et al* [32] have shown strong evidence for a gradual onset of deformation throughout the transitional region. The authors of [32] proposed the coexistence of a spherical configuration, which becomes weakly deformed with increasing $N$, and a deformed configuration, which first appears as a weakly deformed excited state at $N = 57$ and becomes steadily more deformed up to a point of saturation at $N \sim 62$–$64$. Shape coexistence is predicted to extend up to $N = 63$, with the deformed configuration becoming the ground state at $N = 60$ and producing the observed shape change. The trends in the mean square charge radii shown in figure 5, appear to be consistent with this idea of a gradual increase in deformation.

Figure 7 shows the systematics of the first excited $2^+$ state energies, and the energy ratios of the first excited $4^+$ and $2^+$ states, $\mathrm{E}(4_1^+)/\mathrm{E}(2_1^+)$. The $\mathrm{E}(4_1^+)/\mathrm{E}(2_1^+)$ ratio tends to the rotational limit for $N \geqslant 60$, thus supporting the idea of a rigid, well deformed nuclear shape.

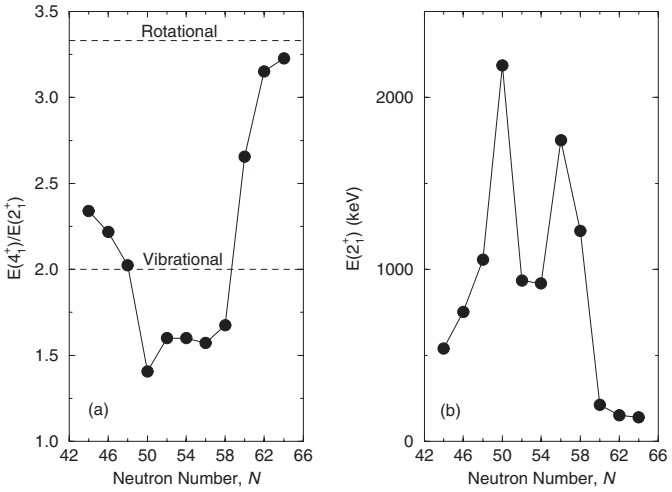


**Figure 7.** (a) Energy ratios of first excited $4^+$ and $2^+$ states, $E(4_1^+)/E(2_1^+)$, plotted against neutron number. The dashed lines indicate the limits of vibrational and rotational motion. (b) First excited $2^+$ state energies, $E(2_1^+)$, against neutron number.

The onset of deformation is equally clear in the course of the $E(2_1^+)$ energies, where a rapid lowering in energy is observed for $N \geqslant 60$. The sharp peaks in the $2^+$ energy at $N = 50$ and $N = 56$ show the stabilizing effects of the neutron shell and sub-shell closures, which are also evident in the $E(4_1^+)/E(2_1^+)$ ratio. The combination of the $N = 56$ and $Z = 40$ sub-shell closures is believed to be responsible for delaying the onset of deformation in zirconium [39], thus producing the rapid shape changes which are observed. On the neutron-deficient side, the $E(4_1^+)/E(2_1^+)$ ratios suggest vibrational behaviour, which is consistent with a softening of the nuclear shape in this region and agrees with the systematics of figure 6.

## 5. Summary and conclusions

Hyperfine structures and isotope shifts were measured for the radioactive isotopes and isomers of zirconium, $^{87,87m,88,89,89m,97-102}$Zr. Nuclear moments, spins and mean square charge radii were extracted from the data.

The changes in mean square charge radii display a kink at $N = 50$, corresponding to the neutron shell closure, and a sharp increase at $N = 60$, where the shape change occurs. Current models [34, 35] were shown to be inadequate in reproducing the observed trends, which are almost identical to those seen in the neighbouring strontium isotope chain.

The magnetic moments of the odd isotopes and isomers were discussed in terms of the single-particle predictions of the shell model, where the isomers involve single particle excitations from $2p_{1/2}$ states. However, no quantitative explanation can be offered for the unexpectedly large magnetic moment of $^{89m}$Zr, which is greater than both the single-particle value and the isotone $^{87m}$Sr.

The quadrupole deformation parameters extracted from the mean square charge radii and quadrupole moments suggest that the zirconium nuclei have soft, vibrational shapes below $N = 50$, where there is a large dynamical contribution to the deformation. Beyond $N = 60$, the data show the nuclei taking on rigid, statically deformed shapes, which are consistent with gamma-ray observations of deformed rotational bands in this region. The trends in mean

square charge radii are compatible with the suggestion of two coexisting shapes for $N > 56$, which become gradually more deformed through the region of the shape change. Discrepancies between deformations derived from mean square charge radii and B(E2) measurements are due to model approximations in the analysis, and may indicate that there are significant changes in the surface diffuseness between isotopes.

Future optical measurements of the long-lived isotopes, $^{93,95}$Zr, are planned in order to improve the systematics in the transitional region. Further plans include the study of more neutron-deficient isotopes, where a reversal of the normal odd–even stagger has been observed below $N = 46$ in the neighbouring chains of strontium [4], krypton [33] and rubidium [5]. In addition, the magnetic moment of $^{85}$Zr is of particular interest due to the presence of an anomalous coupling state in the isotone, $^{83}$Sr [40]. In analogy with $^{83}$Sr, $^{85}$Zr has a nuclear spin of $I = 7/2$ and is expected to show similar coupling. Plans are also in place to study the neutron-deficient and neutron-rich isotopes of yttrium ($Z = 39$), which will further improve the systematics of the $Z \sim 40$ region.

## Acknowledgments

This work has been supported by the UK Engineering and Physical Sciences Research Council, the Academy of Finland under the Finnish Centre of Excellence Programme 2000-2005 (project no 44875) and by the European Union Fifth Framework Programme 'Improving Human Potential—Access to Research Infrastructure', contract no HPRI-CT-1999-00044.

## References

[1] Otten E W 1989 *Treatise on Heavy-Ion Science* vol 8 ed D A Bromley (New York: Plenum) pp 517–638
[2] Billowes J and Campbell P 1995 *J. Phys. G: Nucl. Part. Phys.* **21** 707
[3] Heyde K 1988 *Nuclear Structure of the Zirconium Region* ed J Erbeth, R Meyer and K Sistemich (Berlin: Springer)
[4] Buchinger F *et al* 1990 *Phys. Rev.* C **41** 2883
[5] Thibault C et al 1981 *Phys. Rev.* C **23** 2720
[6] Cooke J 1996 *PhD Thesis* The University of Birmingham
[7] Campbell P, Billowes J and Grant I S 1997 *J. Phys. B: At. Mol. Opt. Phys.* **30** 4783
[8] Äystö J 2001 *Nucl. Phys.* A **693** 477
[9] Levins J M G *et al* 1999 *Phys. Rev. Lett.* **82** 2476
[10] Nieminen A *et al* 2001 *Nucl. Instrum. Methods* A **469** 244
[11] Campbell P *et al* 2002 *Phys. Rev. Lett.* **89**
[12] Forest D H *et al* 2002 *J. Phys. G: Nucl. Part. Phys.* **28** L63
[13] Dendooven P 1997 *Nucl. Instrum. Methods* B **126** 182
[14] Yeandle G *et al* 2000 *J. Phys. G: Nucl. Part. Phys.* **26** 839
[15] Taskinen P *et al* 1989 *Nucl. Instrum. Methods* A **281** 539
[16] Billowes J *et al* 1997 *Nucl. Instrum. Methods* B **126** 416
[17] Billowes J 2001 *Nucl. Phys.* A **682** 206c
[18] Nieminen A *et al* 2002 *Phys. Rev. Lett.* **88** 094801
[19] Gerstenkorn S and Luc P 1978 *Atlas du Spectre D'Absorption de la Molecule de l'Iode 14800–20000 cm*$^{-1}$ (Paris: Centre National de la Recherche Scientifique)
[20] Kopferman H 1958 *Nuclear Moments* (New York: Academic)
[21] Büttgenbach S 1984 *Hyperfine Interact.* **20** 1
[22] King W 1984 *Isotope Shifts in Atomic Spectra* (New York: Plenum)
[23] Griffith J A R *et al* 1979 *J. Phys. B: At. Mol. Opt. Phys.* **12** L1
[24] Griffith J A R, Isaak G R, New R and Ralls M P 1981 *J. Phys. B: At. Mol. Opt. Phys.* **14** 2769
[25] Fricke G *et al* 1995 *At. Data Nucl. Data Tables* **60** 177
[26] Raghavan P 1989 *At. Data Nucl. Data Tables* **42** 189
[27] Pyykkö P 2001 *Mol. Phys.* **99** 1617

[28] Myers W D and Schmidt K H 1983 *Nucl. Phys.* A **410** 61
[29] Berdichevsky D and Tondeur F 1985 *Z. Phys.* A **322** 141
[30] Raman S *et al* 1987 *At. Data Nucl. Data Tables* **36** 1
[31] Lhersonneau G *et al* 1994 *Phys. Rev.* C **49** 1379
[32] Urban W *et al* 2001 *Nucl. Phys.* A **689** 605
[33] Keim M *et al* 1995 *Nucl. Phys.* A **586** 219
[34] Möller P, Nix J R, Myers W D and Swiatecki W J 1995 *At. Data Nucl. Data Tables* **59** 185
[35] Lalazissis G A, Raman S and Ring P 1999 *At. Data Nucl. Data Tables* **71** 1
[36] Artna-Cohen A 1993 *Nucl. Data Sheets* **70** 85
[37] Berkes I *et al* 1992 *Hyperfine Interact.* **75** 93
[38] Mach H 1991 *Nucl. Phys.* A **523** 197
[39] Ragnarsson I 1984 *Phys. Scripta* **29** 385
[40] Anselment M 1987 *Z. Phys.* A **326** 493